Bull. Mater. Sci., Vol. 39, No. 5, September 2016, pp. 1139–1145. © Indian Academy of Sciences.
DOI 10.1007/s12034-016-1239-2

Electrical and magneto transport properties of $La_{0.8-x}Ca_xSr_{0.1}Ag_{0.1}MnO_3$ ($x = 0.1, 0.2, 0.3$)

P SUBHASHINI[1,*], B MUNIRATHINAM[2], M KRISHNAIAH[1], R VENKATESH[3], D VENKATESWARLU[3] and V GANESAN[3]

[1]Department of Physics, Sri Venkateswara University, Tirupati, India
[2]NDT/SPP, SDSC SHAR, Sriharikota, India
[3]Low Temperature Laboratory, UGC-DAE Consortium for Scientific Research, Indore 452001, India

MS received 5 January 2016; accepted 10 March 2016

Abstract. **Lanthanum-based manganites $La_{0.8-x}Ca_xSr_{0.1}Ag_{0.1}MnO_3$ ($x = 0.1, 0.2, 0.3$) doped with both alkaline metal (Ag) and alkaline earth (Ca and Sr) elements are studied. The structural characterization of polycrystalline samples synthesized through low temperature nitrate route confirms orthorhombic structure for all the investigated samples. The morphology of crystal grains shows that the grains are nearly uniform in size and spherical. Electrical resistivity of samples reveal two transition peaks typical of Ag-doped lanthanum-based manganites. Significant room temperature magneto resistivity (MR) is observed for all the samples. MR is found to behave almost linearly with temperature for $x = 0.1$ sample for different magnetic field strengths in contrast to plateau type behaviour observed for $x = 0.3$ sample. Standard temperature-dependent resistivity models such as small polaron and variable range hopping are used to fit the resistivity data in the high temperature range. In the low temperature domain, the resistivity data could be fitted to a model which combines electron–electron scattering and weak localization.**

Keywords. **X-ray diffraction; colossal magneto resistivity; phase separation; weak localization; variable range hopping.**

1. Introduction

Synthesis and characterization of newer and exotic materials are on the phenomenal rise in recent years for potential applications such as magnetic sensing, magnetic storage, magnetic refrigeration, etc. In this context, the La-based manganites $La_{1-y}A_yMnO_3$, where A is a divalent element (e.g., Ca^{2+}, Sr^{2+}, Ba^{2+}) [1–4] have been studied extensively due to a number of interesting physical properties including metal–insulator (MI) transition, colossal magneto resistivity (CMR), charge ordering (CO), orbital ordering, phase separation, etc.

$La_{1-y}Ca_yMnO_3$ (LCMO) has attracted wide attention due to its significant CMR effect and intermediate bandwidth. For $y = 0$ (i.e., $LaMnO_3$), there are four 3d electrons on every manganese ion and the hopping of e_g electron is restricted by the on-site Coulomb repulsion and strong Hund's coupling. The e_g electrons interact with each other by virtual hopping onto neighbouring atoms when their spins are anti-parallel and this super exchange interaction leads to A-type anti-ferromagnetic (AFM) order. For $0.2 < y < 0.5$, the low-temperature ground state is a ferromagnetic metal (FM) and there is a good overlap between Mn d-orbitals and oxygen p-orbitals resulting in high probability of hopping and the e_g carriers become a delocalized electron gas. In this doping range, double-exchange (DE) mechanism and strong electron–lattice coupling are believed to cause metal–insulator transition apart from ferromagnetism and CMR [5]. Two transitions are observed on cooling for $y = 0.5$ composition: (i) paramagnetic to ferromagnetic (FM) state at about 230 K and transition to AFM state occurs at about 135 K on cooling and 185 K on warming [6]. In addition, coexistence of FM and CO phases is widely reported in the samples of $La_{0.5}Ca_{0.5}MnO_3$ [7].

It is known that the overlap between Mn 3d-orbitals and oxygen 2p-orbitals forms the electronically active band, and this overlap can be strongly influenced by the internal pressure generated by the A-site substitution with ions of different radii [8–10]. Specifically, the average radius $\langle r_A \rangle$ of A-site cations is known to induce deformation in unit cell structure and cause rotation and distortion of MnO_6 octahedra to affect not only bandwidth of e_g electrons of Mn ions, but also different electronic phases of above materials. Increasing $\langle r_A \rangle$ by substitution of suitable elements widens the e_g electron band width and enhances Curie temperature (T_C). In addition, the compounds tend to be predominantly FM and metallic with the increase of $\langle r_A \rangle$. The magneto resistivity (MR) is dominantly exhibited near T_C at which there is ferromagnetic order of Mn spins accompanied by a large increase in electrical conductivity. Decreasing $\langle r_A \rangle$ on the other hand is found to decrease T_C and increase MR value drastically. Apart from the size of A-site dopant ions, dopant percentage, oxygen stoichiometry, temperature, magnetic field, electric field, pressure, etc., also play a vital role

*Author for correspondence (subhashinisvu@gmail.com)

in affecting the MR properties [11,12]. When the La^{3+} ions are partially replaced with the monovalent ions such as Na^{+}, Ag^{+}, etc., two Mn^{3+} ions are converted to Mn^{4+} ions for every monovalent ion substitution. This increases in turn the mobility of charge carriers leading to a possible metallic ground state. Among the monovalent-doped manganites, the ones doped with high conducting silver (Ag) ions provide easy conduction paths among the grains resulting in a relatively lower resistivity [13,14] for the samples. In the present paper, we report the synthesis of $La_{0.8-x}Ca_xSr_{0.1}Ag_{0.1}MnO_3$ ($0.1 \leq x \leq 0.3$) manganites and investigation of their electrical and magneto transport behaviours as a function of both temperature and magnetic fields.

2. Experimental

The synthesis of $La_{0.8-x}Ca_xSr_{0.1}Ag_{0.1}MnO_3$ (LCSAMO) manganites ($x = 0.1, 0.2, 0.3$) is carried out through low-temperature NO_3 route [15]. 1 M solutions of $La(NO_3)_2{\cdot}6H_2O$, $Ca(NO_3)_2{\cdot}4H_2O$, $Sr(NO_3)_2$, $Ag(NO_3)_2$ and $Mn(CH_3COOH)_2{\cdot}4H_2O$ are separately prepared using distilled water and mixed together in required proportions. The mixed solutions are stirred using magnetic stirrer and evaporated slowly at 80°C to form dark brownish precipitate. These are then allowed to burn at 500°C for 7 h to obtain samples in the form of black fine powder. These soft powder samples are again calcined at 900°C for another 14 h. The pellets obtained from these polycrystalline powders are finally sintered at 900°C for 14 h and allowed to cool to room temperature by switching off the furnace.

X-ray diffraction (XRD) data of the samples are obtained using Philips X-ray diffractometer with CuKα radiation ($\lambda = 1.5406$ Å) in angular steps of 0.02°. The scanning electron microscopy (SEM) of samples is carried out using Carl Zeiss make (model: l EVO ma 15) equipment and the compositions are verified using energy dispersive spectroscopy (EDS) provision available (Oxford instruments Inca penta FET X3) with the equipment. The temperature-dependent electrical and magneto resistivity of the samples are obtained using the Quantum design Physical Property Measurement System (PPMS in the range of 2–350 K and the magnetic field is varied up to 10 T.

3. Results and discussion

3.1 *Structural characterization, morphology and elemental composition*

XRD patterns (figure 1) of the samples recorded at room temperature are analysed with Rietveld's method using FULLPROF program [16] (figure 2). The XRD analysis confirms orthorhombic crystal structure (Pnma space group) for all the samples and the refined lattice parameters are given in table 1. The unit cell volume (V) of samples is found to decrease with increase of Ca percentage. The average crystallite size $\langle d \rangle$ is estimated using the Scherrer's formula [17] after correcting for instrumental contribution to line broadening and the same is found to be in the range of 13–22 nm (table 1). The average A-site ionic radius $\langle r_A \rangle$ is calculated from standard ionic radii data corresponding to nine fold coordination. The value of $\langle r_A \rangle$ is found to decrease with x, while that of distortion factor (σ^2) which is observed to be negligibly small is observed to increase mildly with increase of x. The tolerance factor also is found to decrease with increasing Ca percentage. The Bragg peak appearing at 38°

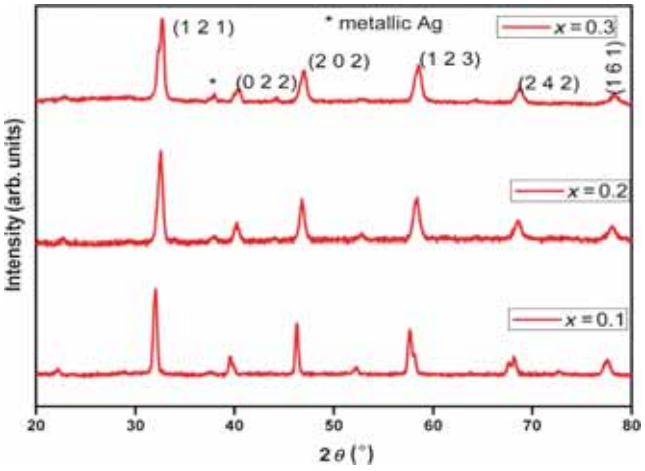

Figure 1. X-ray diffraction patterns of $La_{0.8-x}Ca_xSr_{0.1}Ag_{0.1}MnO_3$ ($0.1 \leq x \leq 0.3$).

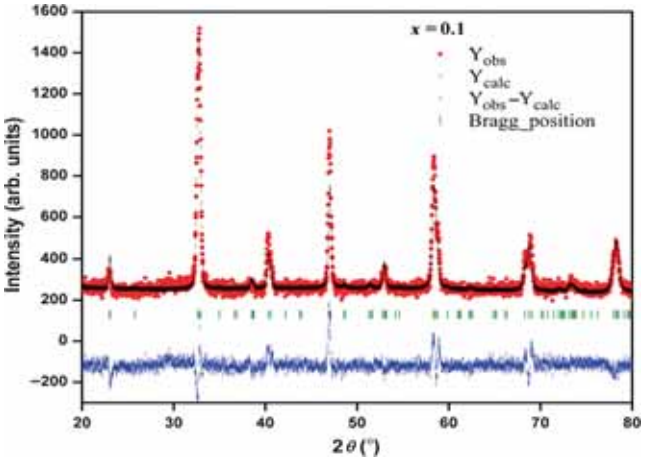

Figure 2. Reitveld refinement pattern for the sample $x = 0.1$.

Table 1. Structural parameters of $La_{0.8-x}Ca_xSr_{0.1}Ag_{0.1}MnO_3$.

Structural parameters	$x = 0.1$	$x = 0.2$	$x = 0.3$
a (Å)	5.434	5.440	5.441
b (Å)	7.709	7.710	7.688
c (Å)	5.487	5.466	5.445
V (Å^3)	229.92	229.25	227.76
$\langle d \rangle$ (nm)	22	14	13
$\langle r_A \rangle$ (nm)	0.1216	0.1212	0.1208
σ^2 (10^{-5} nm^2)	1.76	1.87	1.95
Tolerance factor (t)	0.958	0.957	0.955

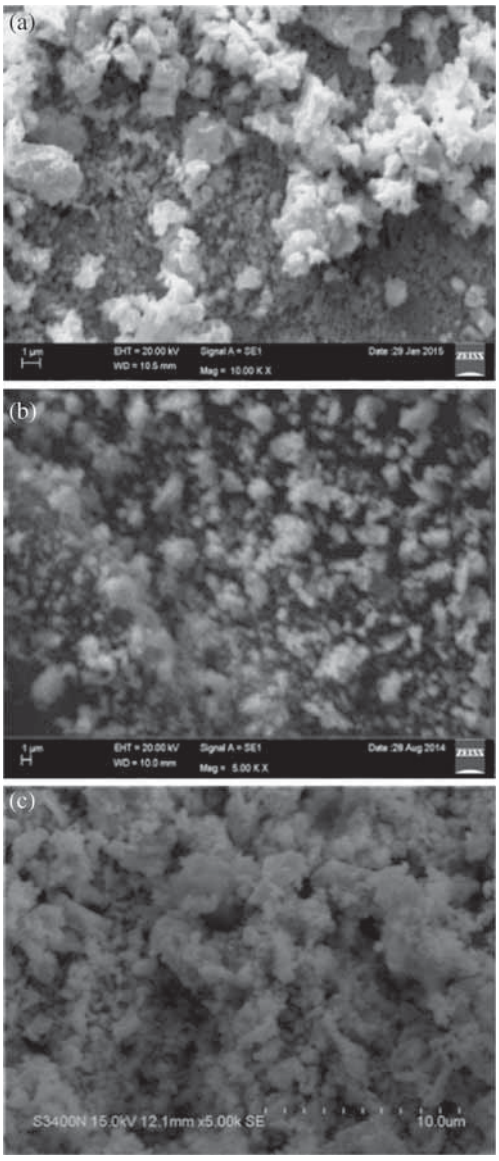

Figure 3. SEM images of $La_{0.8-x}Ca_xSr_{0.1}Ag_{0.1}MnO_3$ ($0.1 \leq x \leq 0.3$).

could be traced to metallic Ag indicating limited solubility of Ag [18,19] and the consequent presence of both the magnetic perovskites and non-magnetic Ag-rich phase in the samples.

SEM images of samples are shown in figure 3. The polycrystalline grains are observed to be near spherical shape and uniform in size. The samples are observed to contain target elements without impurity and the results obtained indicate lesser percentage of calcium as compared to calculated percentage and similar is the case with silver, suggesting the presence of vacancies at A-sites [20].

3.2 *Electrical transport*

Electrical and magnetic properties of monovalent-substituted lanthanum-based manganites have been studied less extensively as compared to divalent substituted systems [21–26] and still lesser for manganite systems which have both

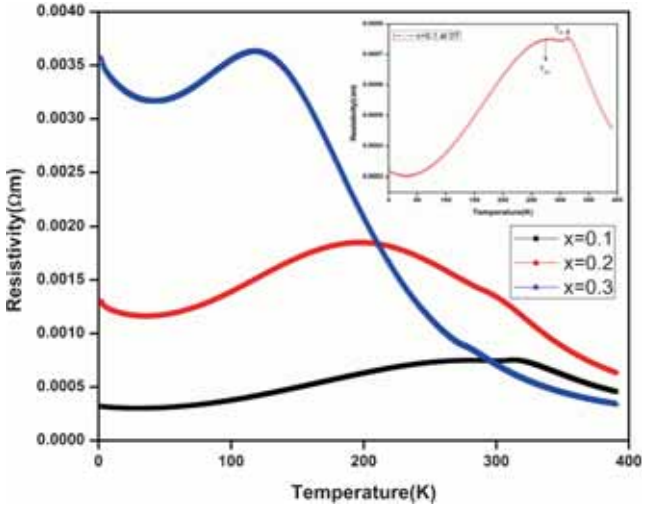

Figure 4. Temperature-dependant electrical resistivity of $La_{0.8-x}Ca_xSr_{0.1}Ag_{0.1}MnO_3$ ($0.1 \leq x \leq 0.3$).

divalent and monovalent substitutions [27–29]. The electrical resistivity of samples as the function of temperature $\rho(T)$ is shown in figure 4.

Two transition peaks are observed in $\rho(T)$ for each sample at T_{p1} and T_{p2} as the temperature is lowered from 380 K. The small peak appearing at T_{p1} is found to decrease as the percentage of Ca is increased at the expense of that of lanthanum (313 K for $x = 0.1$, 288 K for $x = 0.2$ and 282 K for $x = 0.3$) and this insulator to metal transition may be attributed to the intrinsic behaviour of the magnetic perovskites [30]. The second broad peak or the hump noticed at $T_{p2} = 280$ K for $x = 0.1$ may be attributed to the phase separation induced by intrinsic chemical inhomogenity [31]. Substitution of Ag^+ ions gives rise to a random distribution of A-site ions and as a result, the e_g electrons are believed to experience inhomogenity as they move through the crystal grains. Moreover, for every monovalent Ag^+ ion substituted for the trivalent La^{3+} ion, two Mn^{3+} ions oxidized to Mn^{4+} ions giving rise to individual regions rich in Mn^{4+} and Mn^{3+}, respectively. This in turn induces electron inhomogeneity and leads to phase separation. Consequent to this, there is creation of ferromagnetic insulating (FMI) and ferromagnetic metallic (FMM) phases in the region of the hump [31]. In addition, when this sample undergoes transition from paramagnetic insulating to ferromagnetic metallic phase with decreasing temperature, the curve $\rho(T)$ does not show pure metallic state due to the simultaneous existence of FMI and FMM phases. However, as the temperature is further lowered, the insulating regions diminish and FMM phase develops better connectivity through the percolation process leading to broad transition at T_{p2}. The same hump is observed to grow higher in resistivity in addition to shifting more towards low temperatures as the x is increased ($T_{p2} = 193$ K for $x = 0.2$ and 118 K for $x = 0.3$). Also, there is a rise in the value of resistivity corresponding to the hump of $x = 0.3$ (i.e., $La_{0.5}Ca_{0.3}Sr_{0.1}Ag_{0.1}MnO_3$) by nearly an order of magnitude as compared to $x = 0.1$ sample. This steep rise may be

attributed more to the transition to the CO phase as has been observed in half-doped lanthanum-based manganite systems than to the effect due to Ag substitution. The decrease of structural parameters, such as unit cell volume, tolerance factor and the average radius $\langle r_A \rangle$ with increase of x (table 1) is also observed to be in line with the increase of resistivity due to the decreasing electronic band width and lesser mobility for electrons.

3.2a *High temperature behaviour*: The variation of electrical resistivity with temperature of both the divalent and monovalent lanthanum-based manganites is usually dominated by polaronic transport in the paramagnetic state of high temperature domain in contrast to ferromagnetic phase of low temperature domain, where various electron scattering processes are observed to determine the resistivity. Regarding the high temperature resistivity behaviour, two mechanisms are proposed in general for the charge transport in manganites, where the carriers are localized. The first process involves hopping of small polarons to the nearest neighbour sites associated with the thermally activated energy known as small polaron model (SPM). In the adiabatic regime, the charge carrier motion is faster than the lattice vibrations and the resistivity expression is given by

$$\rho = AT \exp(E_a/k_B T), \tag{1}$$

where A is the temperature-independent resistivity attributable to scattering by impurities, defects, grain boundaries and domain walls, E_a the activation energy and k_B the Boltzmann's constant. The resistivity data fitted to the SPM model is shown in figure 5a–c and values of A and E_a are given in table 2. The activation energy obtained with this model is found to increase with increase in Ca percentage. In the second process also the charge carriers are localized to the states of nearly equal energy. These states are thought to be located at random distances in the lattice of each grain due to the randomness in the potential. This mechanism of electron hopping between states is called variable range hopping (VRH) model and is expressed as

$$\rho = \rho_\infty \exp[(T_o/T)^{1/4}], \tag{2}$$

where ρ_∞ is the temperature-independent parameter and T_o the characteristic temperature [32]. The fitting of resistivity data with VRH model is also shown in figure 5a–c and the estimated values of ρ_∞ and T_o values are shown in table 2. The increase of T_o with the increase of x, points to the enhancement of carrier effective mass or narrowing of the e_g electron band width and the rise in the value of resistivity [33]. Comparing the performances of the above two models in fitting the resistivity data, the VRH model is found to capture the transport behaviour marginally better than the small polaron model in the high-temperature paramagnetic domain.

3.2b *Low temperature behaviour*: The observation of minimum resistivity in the low-temperature domain and the subsequent rise in resistivity of the samples as the temperature is further reduced are seen to be similar to that reported in a number of materials in recent years [34–36]. Various models have been proposed to explain this anomalous behaviour at low temperature [33,37,38]. For the present samples, the following model which combines the weak localization and electron–electron scattering

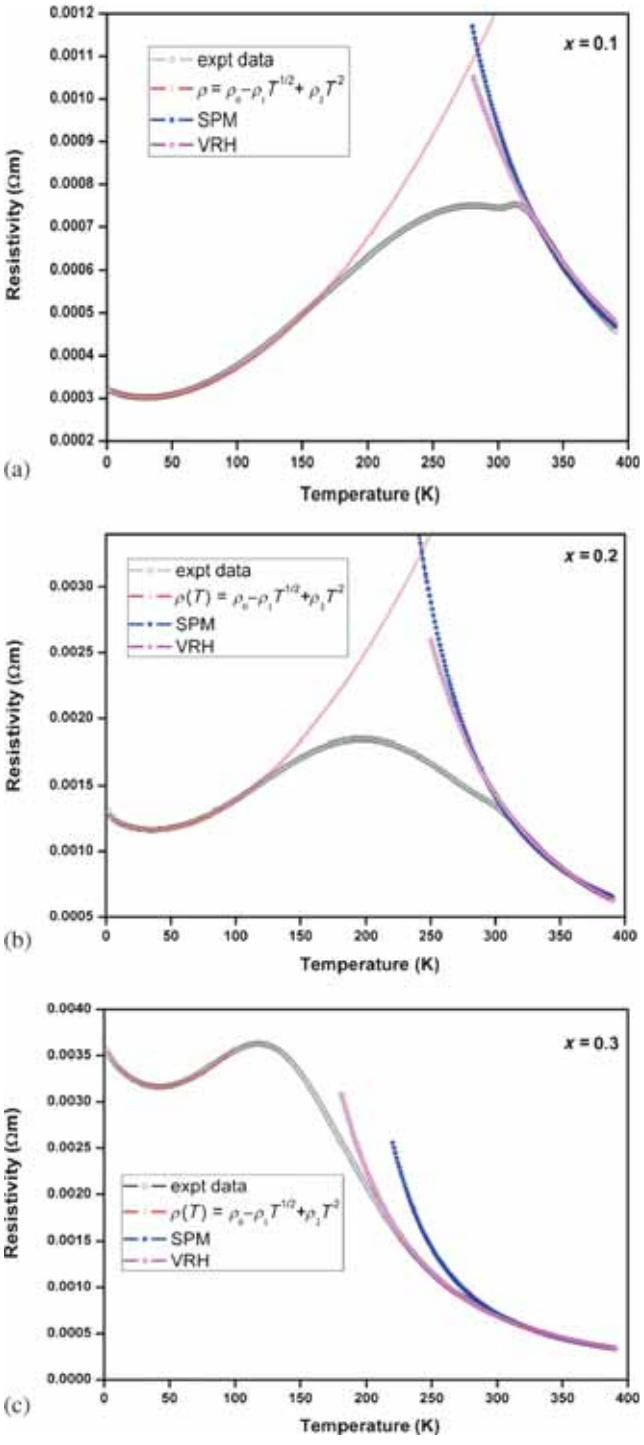

Figure 5. (**a–c**) Temperature-dependent resistivity of $La_{0.8-x}Ca_xSr_{0.1}Ag_{0.1}MnO_3$ ($0.1 \leq x \leq 0.3$) in zero field, where solid lines are the fitting graphs for different models.

Table 2. Fitting parameters obtained from different models.

Model parameters	$x = 0.1$	$x = 0.2$	$x = 0.3$
Low temperature region			
ρ_0 (Ωm)	3.28×10^{-4}	13.30×10^{-4}	37.20×10^{-4}
ρ_1 (Ωm K$^{-1/2}$)	6.70×10^{-6}	3.64×10^{-5}	1.13×10^{-4}
ρ_2 (Ωm K^{-2})	1.13×10^{-8}	4.23×10^{-8}	9.86×10^{-8}
Small polaron model			
A (Ωm K^{-1})	5.08×10^{-8}	5.37×10^{-8}	3.02×10^{-8}
E_a (eV)	0.1	0.11	0.11
VRH model			
ρ_∞ (Ωm)	5.23×10^{-8}	1.33×10^{-9}	5.06×10^{-9}
T_o (K)	2.68×10^{6}	5.30×10^{6}	5.91×10^{6}
$1/\alpha$ (Å)	6.97	5.55	5.33
R (Å) at 300 K	25.44	24.01	23.72
E_v (eV) at 300 K	0.06	0.07	0.08

mechanisms [14] is found to fit the resistivity data well for ($T < T_P$),

$$\rho(T) = \left\{ \frac{1}{a + bT^{1/2}} \right\} + \rho_2 T^2, \tag{3}$$

where the first term is linked to the weak localization effect, a is a temperature-independent residual conductivity and b the diffusion constant. The second term ρ_2 represents the resistivity due to electron–electron scattering. Expanding the first term binomially and rewriting the above equation with $\rho_0 = 1/a$ and $\rho_1 = -b/a^2$, we have

$$\rho(T) = \rho_0 - \rho_1 T^{1/2} + \rho_2 T^2. \tag{4}$$

The best fit parameters are given in table 2. It can also be seen from figure 5 that the theoretical and experimental points match very well indicating that the anomalous resistivity behaviour at low temperature is in corroboration with the above models.

3.3 *Magneto transport*

Temperature-dependent electrical resistivity of the samples for different magnetic field strength is shown in figure 6a–c. The first peak at T_{p1} is found to disappear for all the samples as the magnetic field is increased. The hump observed at T_{p2} is observed to shift to higher temperatures with the increase of magnetic field. With the increase of magnetic field, the resistivity $\rho(T)$ is found to decrease significantly as e_g carriers suffer less scattering during the hopping process due to favourable alignment of spins at Mn sites.

The MR of the samples is estimated using the following formula

$$\mathrm{MR} = \frac{\rho(T, H) - \rho(T, H = 0)}{\rho(T, H = 0)} \times 100\%, \tag{5}$$

where $\rho(T, H)$ and $\rho(T, H = 0)$ are the resistivity of samples measured in applied and zero magnetic fields, respectively. MR as a function of temperature for different magnetic fields is shown in figure 6a–c. The value of MR is found to increase as the temperature is lowered attaining the maximum at the lowest measured temperature (2 K). At $T = 2$ K and in magnetic field of 3 T, the MR value is found to be 33% for $x = 0.1$, 36% for $x = 0.2$ and 39% for $x = 0.3$ and the MR value jumps to 47% ($x = 0.1$), 54% ($x = 0.2$) and 68% ($x = 0.3$) at 10 T. The interesting aspect of this increase of MR with the field is the attainment of local maximum close to the first peak (T_{p1}) of the samples. For instance, the values of MR for $x = 0.2$ sample close to the room temperature (300 K) for different field strengths are as follows: 9% at 3 T; 14% at 5 T; 21% at 8 T; 25% at 10 T.

It is known that MR arises due to the contributions of both the grains (intrinsic) as well as the grain boundaries (extrinsic) in polycrystalline manganites. The MR in the region close to T_{p1} is believed to arise from the grains and that at lower temperatures arises due to grain boundaries. The mechanism of spin-polarized tunnelling of carriers through grain boundaries is usually attributed to the cause of extrinsic MR [39]. The transport across the grain boundaries is observed to be relatively sensitive to the applied field. At zero fields, because of different orientations of opposite spins, an energy gap is generated between the charge carriers of neighbouring grains. Application of external magnetic field forces the grains to orient such that the carrier spins from the neighbouring grains align favourably to reduce the energy gap [19,40]. Also, the gradual flattening of the resistivity minimum at low temperature with increase in magnetic field is attributed to the above mechanism.

Another interesting behaviour of MR is its proportional variation with temperature for $x = 0.1$ in the temperature range from 60 K to about 300 K (figure 6a–c). This linear variation of MR is a typical characteristic of a granular system wherein the spin-dependent electron tunnelling process dominates across the grain boundaries [14]. In the above temperature range, the rate of change of MR for $x = 0.1$ composition is found to attain a maximum value of 0.1%

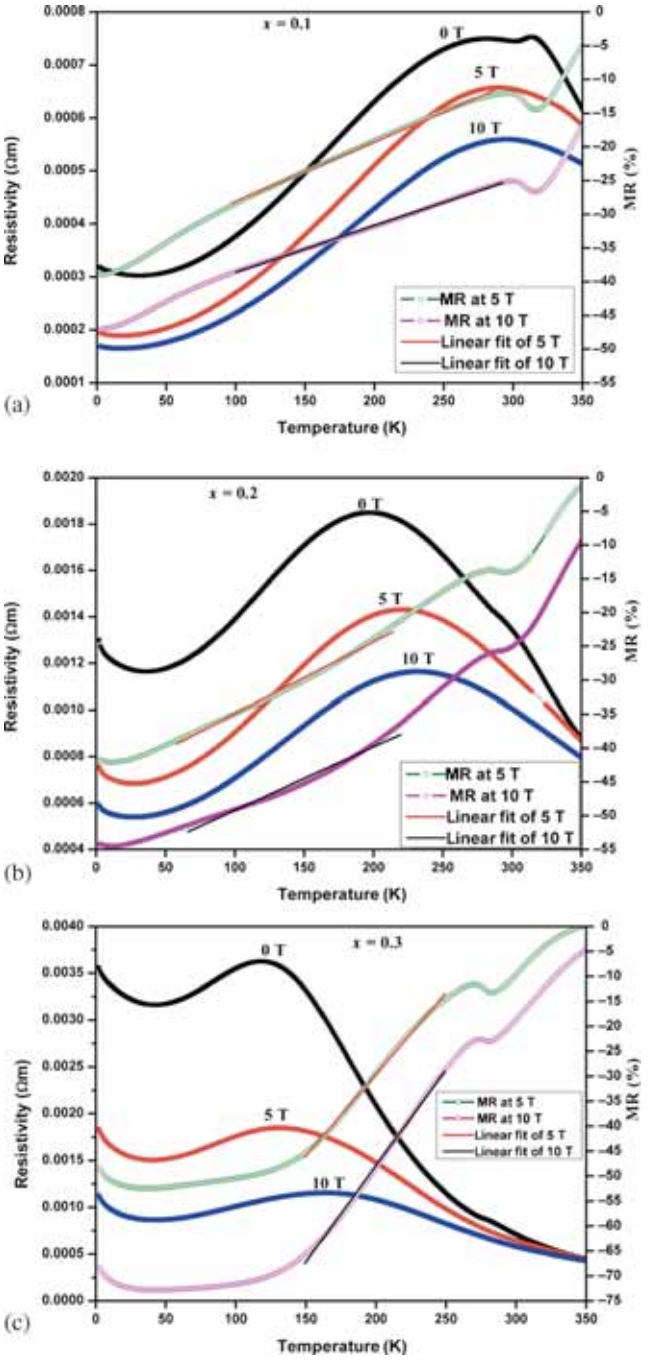

Figure 6. (**a–c**) Temperature-dependent resistivity, magneto resistiity and its proportional behaviour at different magnetic fields.

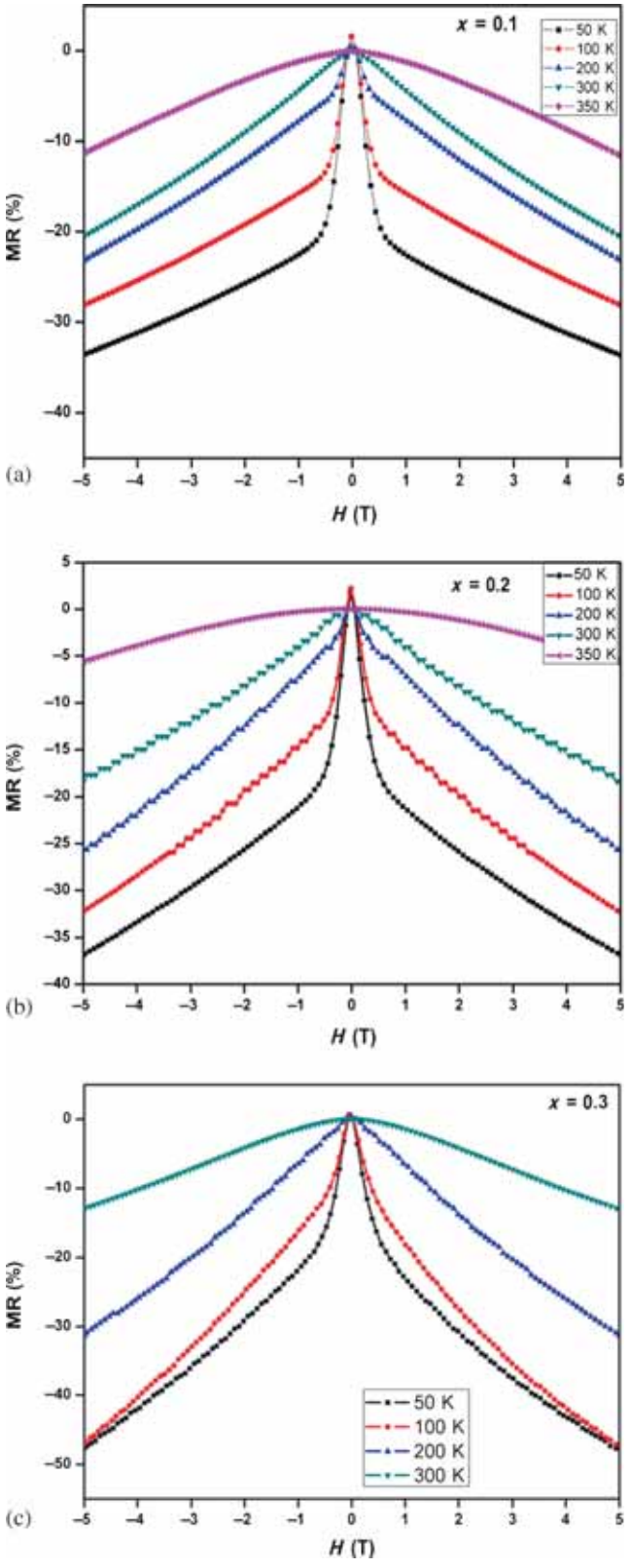

Figure 7. (**a–c**) MR as a function of magnetic field at different temperatures.

per unit Kelvin at 3 T and then decreases to 0.07% per unit Kelvin at 10 T. The same proportional behaviour of MR is also observed for $x = 0.2$ sample, but only up to 3 T and thereafter it undergoes a gradual transition to non-proportional behaviour for larger fields. In contrast to the above, the behaviour of MR turns into a plateau type for $x = 0.3$, specifically in the low temperature range from 2 K to about 150 K, attaining about 38% for 3 T, 52% for 5 T; 66% for 8 T and 73% for 10 T. To examine the characteristics of MR as a function magnetic field, the latter is varied continuously from −5 T to 5 T at different temperature values. From figure 7a–c, it is clear that MR exhibits nearly symmetrical behaviour at the zero field. It is also interesting

to observe the steep increase of MR at low magnetic fields (<1 T) when the temperature of the samples is lowered. This steep increase is observed to be maximum for $x = 0.1$ sample at $T = 50$ K.

4. Conclusion

The electrical and magneto transport properties of $La_{0.8-x}Ca_xSr_{0.1}Ag_{0.1}MnO_3$ ($x = 0.1, 0.2, 0.3$) manganites are investigated. The limited solubility of Ag is revealed in the XRD analysis for all the samples prepared through low-temperature route. The temperature-dependent electrical resistivity $\rho(T)$ of samples shows two transition peaks, a typical characteristic of Ag-doped lanthanum-based manganites. In the high-temperature range, the VRH model is found to simulate the resistivity behaviour marginally better as compared to small polaron model. The anomalous low temperature behaviour is explained in terms of a model which combines electron–electron scattering and weak localization. The study of magneto transport behaviour reveals significant magneto resistivity at room temperature which can be exploited for magnetic sensing applications.

Acknowledgement

We are thankful to UGC-DAE CSR, Indore, India, for providing MR facilities. One of the author, PS is grateful to University Grant Commission, New Delhi, India, for the grant of Rajiv Gandhi national fellowship.

References

[1] Jonker G H and van Santen J H 1950 *Physica* **16** 337

[2] Wollan E O and Koehler W C 1955 *Phys. Rev*. **100** 545

[3] Jin S, Tiefel T H, McCormack M, Fastnacht R A, Ramesh R and Chen L H 1993 *Science* **264** 413

[4] Schiffer P, Ramirez A P, Bao W and Cheong S W 1995 *Phys. Rev. Lett.* **75** 3336

[5] Tokura Y (ed.) 2000 *Colossal magneto resistance oxides* (London: Gordon and Breach)

[6] Dho J, Kim I, Lee S, Kim K H, Lee H J, Jung J H and Noh T W 1999 *Phys. Rev. B* **59** 492

[7] Loudon J C, Mathur N D and Midgley P A 2002 *Nature* **420** 797

[8] Neumeier J J, Hundley M F, Thompson J D and Heffner R H 1995 *Phys. Rev. B* **52** 7006

[9] Hwang H Y, Cheong S W, Radaelli P G, Marezio M and Batlogg B 1995 *Phys. Rev. Lett.* **75** 914

[10] Radaelli P G, Iannone G, Marezio M, Hwang H Y, Cheong S W, Jorgensen J D and Argyriou D N 1997 *Phys. Rev. B* **56** 8265

[11] Coey M D and Viret M 1999 *Adv. Phys.* **48** 167

[12] Dogotto E, Hotta T and Moreo A 2001 *Phys. Rep.* **344** 1

[13] Battabyal M and Dey T K 2004 *J. Phys. Chem. Solids* **65** 1895

[14] Kalyana Lakshmi Y and Venugopal Reddy P 2009 *J. Magn. Magn. Mater.* **321** 1240

[15] Pai M R, Wani B N and Bharadwaj S R 2006 *J. Indian Chem. Soc.* **83** 336

[16] Tripathi R, Awana V P S *et al* 2009 *J. Phys. D Appl. Phys*. DOI: 10.1088/0022-3727/42/17/175002

[17] Cullity B D 1977 *Elements of X-ray diffraction* (Boston, MA: Addition-Wesley Publishing co.)

[18] Tang T, Gu K M, Cao Q Q, Wang D H, Zhang S Y and Du Y W 2000 *J. Magn. Magn. Mater.* **222** 110

[19] Gencer H, Pektas M *et al* 2012 *J. Magnet.* **17** 176

[20] Pekala M *et al* 2005 *J. Magn. Magn. Mater.* **290** 928

[21] Itoh I M *et al* 1995 *Phys. Rev. B* **12** 522

[22] Rao G H *et al* 1997 *Appl. Phys. Lett.* **70** 1900

[23] Tao T *et al* 2000 *Appl. Phys. Lett.* **77** 723

[24] Chen C C *et al* 1997 *Appl. Phys. Lett.* **71** 1424

[25] Horyn R *et al* 2002 *J. Alloys Compnd.* **383** 80

[26] Ye S L *et al* 2001 *J. Appl. Phys.* **90** 2943

[27] Koubaa M, Cheikhrouhou Koubaa W and Cheikhrouhou A 2009 *Phys. Procedia* **2** 997

[28] Cherif B, Rahmouni H, Smari M, Dhahri E, Moutia N and Khirouni K 2015 *Physica B* **457** 240

[29] Kim J S, Ulyanov A N, Kang Y M, Min S G, Yu S C and Yoo S I 2007 *J. Magn. Magn. Mater.* **310** 2818

[30] Yuan X-B, Liu Y-H, Huang B-X, Wang C-J and Mei L-M 2005 *Solid State Commun.* **135** 170

[31] Battabyal M and Dey T K 2004 *Solid State Commun.* **131** 337

[32] Munirathinam B, Krishnaiah M, Devarajan U, Esakki Muthu S and Arumugam S 2012 *J. Phys. Chem. Solids* **73** 925

[33] Venkataiah G and Venugopal Reddy P 2005 *Solid State Commun.* **136** 114

[34] Rozenberg E, Auslender M, Felner I and Gorodetsky G 2000 *J. Appl. Phys.* **88** 2578

[35] Auslender M, Kar'kin A E, Rozenberg E and Gorodetsky G 2001 *J. Appl. Phys.* **89** 6639

[36] Sarkar T, Ghosh B, Chatterji T and Raychaudhuri A K 2008 *Phys. Rev. B* **77** 235112

[37] Lalitha G and Venugopal Reddy P 2010 *J. Alloys Compnd.* **494** 476

[38] Pekala M, Drozd V, Fagnard J F, Vanderbemden P H and Ausloos M 2009 *J. Appl. Phys.* **105** 013923

[39] Helman J S and Abeles B 1976 *Phys. Rev. Lett.* **37** 1429

[40] Battabyal M and Dey T K 2005 *Physica B* **367** 40